Spontaneous Differentiation of human Neural Stem Cells on Nanodiamond

Alice C Taylor[a,1], Citlali Helenes González[b,1], Patrizia Ferretti[b], Richard B Jackman[a]

[a] London Centre for Nanotechnology and Department of Electronic and Electrical Engineering, University College London, 17-19 Gordon Street, London, WC1H 0AH, UK

[b] Stem Cell and Regenerative Medicine Section, UCL Institute of Child Health, University College London, 30 Guilford Street, London, WC1N 1EH, UK

* Corresponding author, r.jackman@ucl.ac.uk

[1] These authors contributed equally to this work

Abstract

The potential use of stem cells in regenerative medicine requires the ability to be able to control stem cell fate as cellular networks are developed. Here, nanodiamonds (~10nm) are supported on glass and shown to be an excellent host for the attachment and proliferation of human neural stem cells. Moreover, it is shown that spontaneous differentiation into neurons occurs on nanodiamonds. The use of variously oxygen terminated and hydrogen terminated nanodiamonds has been explored. It is shown that O–ND monolayers promote the differentiation of hNSCs into neurons with increased total neurite length, degree of branching and density of neurites when compared with H–NDs or the glass control. The total number of neurites and total neurite length expressing MAP2, a protein enriched in dendrites, was over 5 times higher for spontaneously differentiated neurones on the O–NDs compared to the control. The fact that inexpensive nanodiamonds can be attached through simple sonication from water on 2D and 3D shapes indicates significant promise for their potential as biomaterials in which neuro-regenerative diseases can be studied.

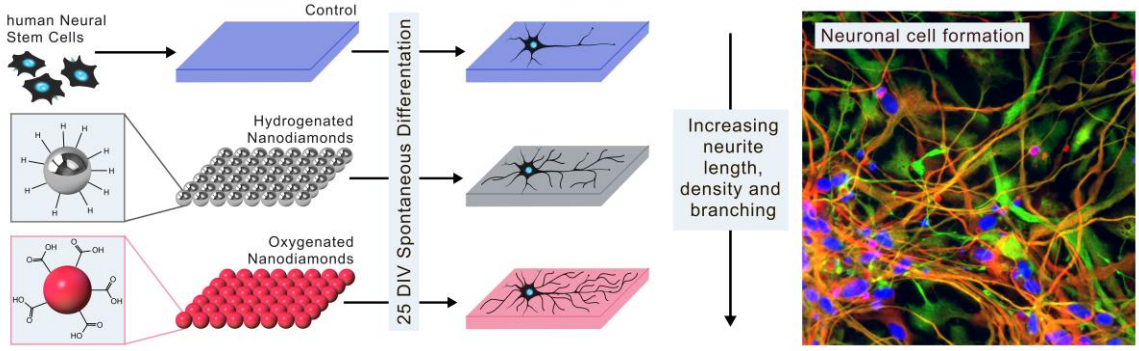

Graphical abstract

The spontaneous differentiation of human Neural Stem Cells (hNSCs) has been investigated on hydrogenated and oxygenated nanodiamond monolayers. After 25 DIV the nature of the differentiated cells are investigated using immunocytochemistry and RT-PCR. Neurite tracing has been performed to statistically highlight differences in neurite length, density and degree of branching.

Keywords

Nanodiamond, human Neural Stem Cells, surface-functionalisation, stem cell differentiation.

Introduction

The global population is rapidly aging, and with this neurodegenerative disease is becoming far more common. Indeed, it is regarded as one of the main threats to the quality of life in the elderly and a significant burden on the provision of global healthcare. Neurodegenerative diseases are acute and chronic conditions, which originate from the death of neurons in the central nervous system (CNS). Conventional treatment for many neurological degenerative diseases may relieve symptoms but rarely terminates the condition [1]. Stem–cell based therapy has the potential to be beneficial for the repair of the CNS through cell replacement and by promoting the survival of affected neurons [2]. The use of human neural foetal tissue in cell–based therapy has been used to treat Parkinson's [3] and Huntington's [4] disease in patients. This approach doesn't provide a practical route to CNS therapeutics due to both the limited availability of human foeti and ethical restrictions. Consequently, extensive research into the use of human neural stem cells (hNSCs) for cell replacement therapies is being undertaken. Stem–cell based therapy is the present standard for the treatment of blood tumours. However, the application of using hNSCs replacement for diseases affecting the CNS is not yet developed and is currently being clinically scrutinised. Despite significant scientific progress since the discovery of hNSCs in 1989 [5], a profound understanding of the basic biology of NSCs is lacking.

Along with increased knowledge, it is imperative that we learn how to manipulate the fate of hNSCs. In order to utilise the potential of stem cells in the field of regenerative medicine, it is essential that we are able to isolate the cells from their natural setting, propagate the cells in culture, and introduce the cells to a foreign environment [6]. To do this, the understanding of how stem cells interact with their natural environment is essential; such environments are termed the stem cell 'niche'. The niche controls stem cell fate [7] through signalling, and by interacting with the support tissue and the extracellular matrix (ECM) [8]. Upon the removal of stem cells from their *in vivo* niche, they regularly differentiate uncontrollably when subsequently cultured *in vitro.* In order to continue developing stem cell therapies, it is critical that stem cell fate can be controlled outside of its natural environment by replicating conditions *in vitro* using model systems [9,10]. An importance of using model systems is the resultant tractability in testing hypotheses for both biomedical applications and fundamental stem cell biology [11]. In order to recreate the stem cell niche, materials which can be precisely controlled are required, with a broad range of materials being investigated for their stem cell interactions [12-15].

As a cell line, hNSCs offer an irreplaceable resource for studying neurodegenerative diseases, and so it is of uttermost importance that we understand the intra– and extra–cellular mechanisms, which govern the fate of such cells. The central nervous system (CNS) consists of neurons, astrocytes, oligodendrocytes and microglia, all of which are important for maintaining function in the CNS. However, the neuron is often deemed the 'building block' of the CNS due to its role in neurotransmission. Neurons are able to transmit and receive electrical signals, and countless aspects of physiology, behaviour and emotion result from this electrical activity. Therefore, the *in vitro* production of human neurons from hNSCs is fundamental for advances in neuro–regenerative medicine to take place. The potential for expanding foetal derived hNSCs in suspension cultures containing specific growth factors has been explored [16,17]. Growth Factors, which are naturally occurring, stimulate cell survival and proliferation of cells by modulating growth control genes [18]. However, early experiments resulted in the production of neuronal cell neurospheres due to inadequate substrates giving rise to a lack in cellular adhesion. Neurosphere formation is often accompanied by the loss of capacity in which such cells can self-renew and differentiate [19]. Additionally, the identity and quantity of cells inside a neurosphere is heterogenous which provides difficulties in quantifying results [20]. The ideal neural network formation involves highly

branched neurites enabling effective intercellular communication. The long–term differentiation capacity of hNSCs has since been demonstrated [21] and such findings provide a platform in which a range of neurobiological conditions can be studied.

Useful biomaterials must be biocompatible with the prospect of being used to improve function, promote recovery and treat neurological disorders in the CNS. Ideal neural scaffolds are both supportive and bio–active; the engineered tissue should have the capacity to modify function of the implanted cells [22]. In order to greatly improve tissue regrowth in damaged areas of the brain, the biomaterial must induce both endogenous and transplanted NSCs differentiation into neural cells [23]. Diamond has previously been shown to be biocompatible and supportive of neuronal cell growth [24-28]. Nanocrystalline diamond (NCD) films and nanodiamond particles have both been shown to be bio–active [29,30]. NCD films have been shown to support hNSC proliferation and differentiation [31,32]. The interaction of living systems with macroscopic or other nanostructured materials is not comparable [33].

Herein, the use of nanodiamond monolayers for the support of hNSC differentiation has been investigated. The bio–activity of these ND monolayers has also been scrutinised, with their effect on the spontaneous differentiation of hNSCs being examined. The results show that both hydrogen and oxygen functionalised NDs (H–NDs + O–NDs) support the differentiation of hNSCs into neurons, however, attachment, neurite outgrowth and degree of branching significantly higher with the use of O–NDs. Spontaneous differentiation of hNSCs on nanodiamond monolayers yields neuronal cells on both H–NDs and O–NDs; this is the first time this has been observed. Encouraging the differentiation of hNSCs into neurons is important for applications where conditions mimicking the stem cell 'niche' are required. Neurite extension of differentiated neurons was considerably higher on O–NDs, compared to H-NDs, complimenting previous results [27]. The demonstrated capacity of O–NDs for increasing adhesion, encouraging neuronal differentiation and stimulating neuronal network formation, suggests it's promising for use as a biomaterial for neurological applications.

Results

Nanodiamond seeding

Nanodiamond monolayers have been previously shown to induce neuronal adhesion [30]. Here, a monolayer of hydrogenated nanodiamonds acted both as an experimental platform itself and a supply of material that could be subsequently oxygen functionalised. After initial dehydration and hydrogen treatment, nanodiamond power was resuspended in DI water. The resultant colloid suspension was sonicated in a bench top sonicator for 30 minutes. Figure 1 shows (a) dynanmic light scattering (DLS) data for the nanodiamond colloid solution before (orange) and after (blue) ultra-high powered sonication. The corresponding atomic force microscopy (AFM) data shown in part (b) confirms that this has been a successful method of de-agglomerating the aggregates of hydrogenated nanodiamonds and a monolayer of hydrogen-nanodiamonds has been achieved. In all cases the substrate used was glass coverslips.

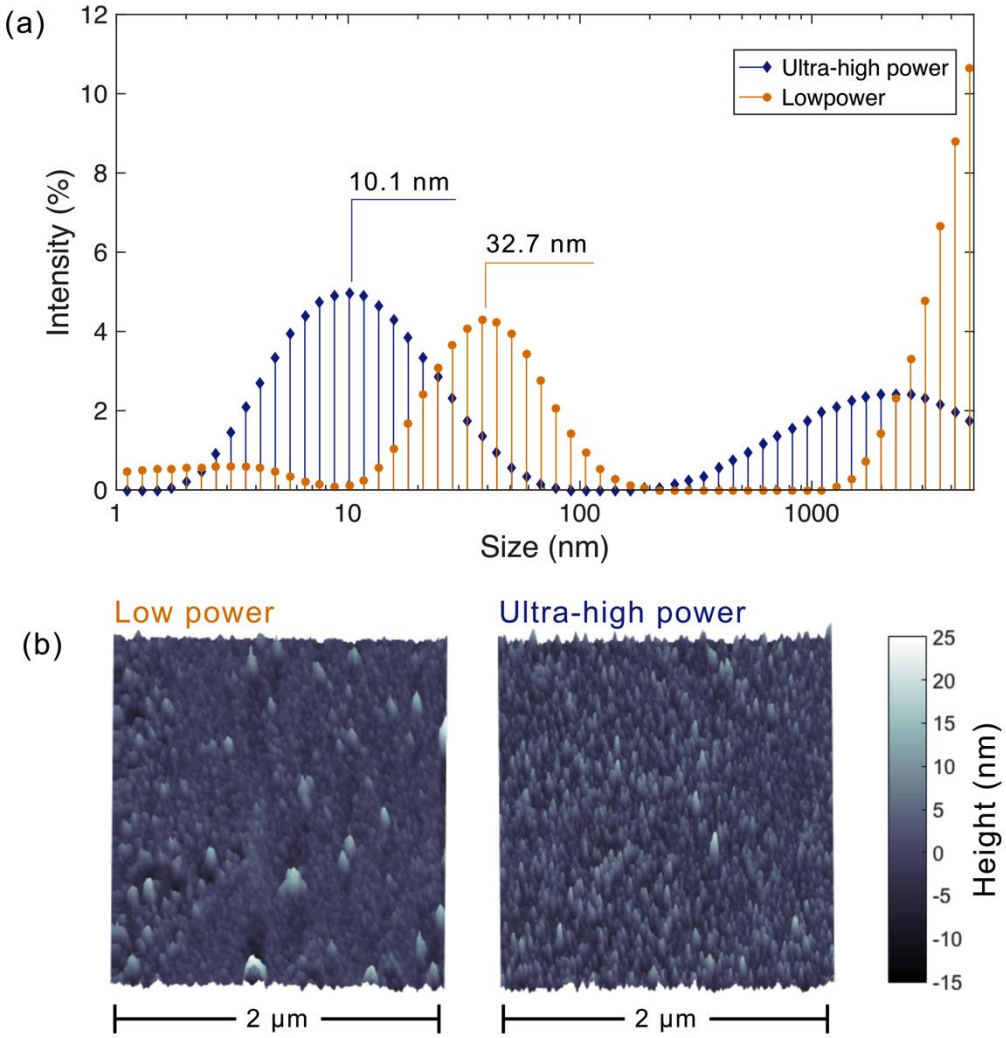

Figure 1 a) Dynamic light scattering data showing the intensity in (%) of the particle size distribution of hydrogenated nanodiamonds re–suspended in DI water before (orange) and after (blue) ultra-high powered sonication for 5 hours. The size of individual nanodiamond particles in 5–10 nm and therefore the sonication results in the de–aggregation of nanodiamond clusters. b) Corresponding Atomic Force Microscopy (AFM) scans of nanodiamonds seeded onto glass before and after sonication. Scan size 2 µm square.

Spontaneous differentiation of hNSCs on nanodiamond monolayers

After 25 DIV without differentiation inducing reagents, hNSCs were fixed and stained with two combinations of fluorescent markers on the control, H– and O–NDs. Figure 2 shows neurons labelled for NF200 (red), MAP2 (green) and Hoechst (blue) which have been spontaneously differentiated on (a) H–and (b) O–NDs, (c) the glass control, (d) and inductively differentiated into neurons on (d) and (e) Tissue Culture Polystyrene (TCPS) control at 25 DIV and 10 PCWs respectively. It can be seen from the fluorescent images of the labelled dendrites in figure 2 that morphology of the neurites which have been spontaneously differentiated very closely resemble neurons in which their differentiated has been controlled.

Figure 3 shows neurons which have been stained for NeuN (green), DCX (red) and Hoechst (blue). The fluorescent images shown in figure 2 and 3 are examples of images which were subsequently used for neurite tracing analysis using the Simple

Neurite Tracer (SNT), a plugin of Fiji software. Statistical analysis was performed using the one–way analysis of variance (ANOVA) test, which is shown in figures 4 and 5.

NF200 is a protein present in neurofilaments and is expressed in mature axons; it is responsible for the regulation of axonal width. MAP2 is a protein associated with the crosslinking of microtubules, and is enriched in dendrites [34,35]. The presence of both MAP2 and NF200 suggests that the spontaneously differentiated hNSCs are neurons, which after 25 DIV are already expressing signs of maturity, comparable to those shown in figure 2 (e), of induced neuronal differentiated cells after 10 post conception weeks (PCW) on the TCPS control. Hoechst is used to stain DNA in the nuclei.

NeuN is expressed in neural cells with significantly more maturity than neural precursor cells. DCX is expressed during the division of immature neural precursor cells. The obvious presence of NeuN on the glass control and both H– and O–NDs implies that the hNSCs have spontaneously differentiated into neurons without the need for any inducing factors being present in the culture medium. The small quantities of DCX expressed on all three substrates suggest that the hNSCs are mature in their development with minimal division of precursor cells occurring.

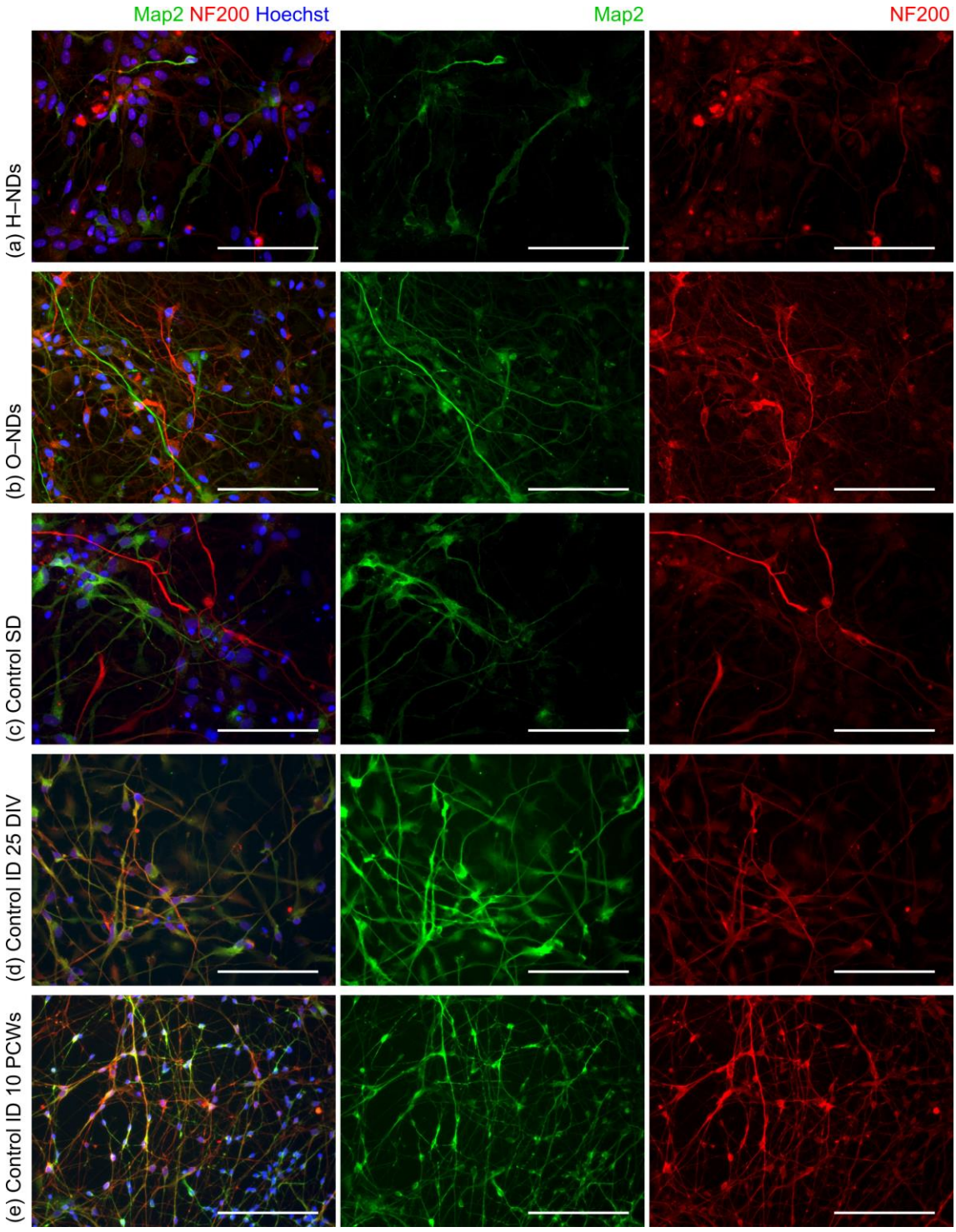

Figure 2 Fluorescently stained images of neurons, which have been differentiated from hNSCs after 25 DIV for (a – d) and 10 Post Conception Weeks (PCWs) (e). (a) Spontaneous differentiation on H–NDs, (b) spontaneous on O–NDs, (c) Spontaneous Differentiation (SD) on the glass Control. (d + e) Induced Differentiation (ID) into neurons on TCPS control after 25 DIV and 10 PCWs respectively. Neurons have been stained using MAP2 (green), NF200 (red) and Hoechst (blue). All scale bars 100 µm, magnification 40x.

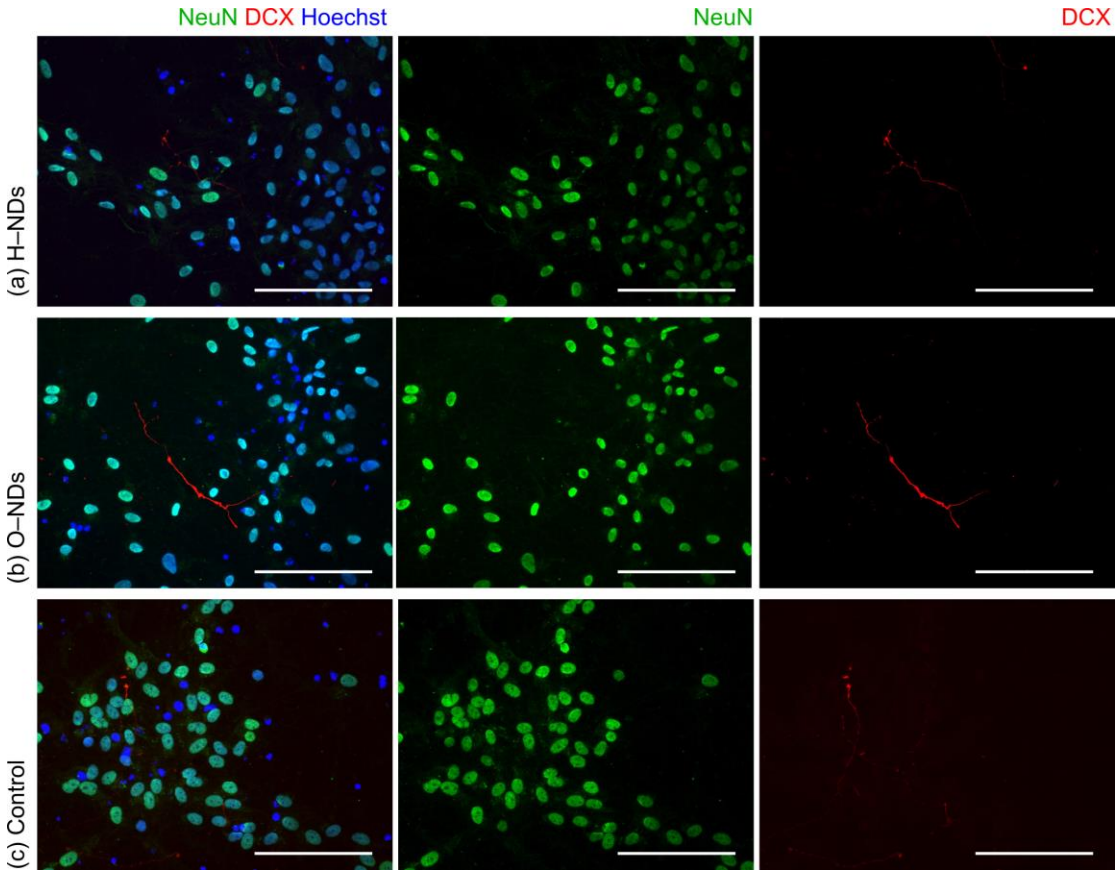

Figure 3 Fluorescently stained images of neurons, which have been differentiated from hNSCs after 25 DIV and (b) NeuN (green), DCX (red) and Hoechst (blue). All scale bars 100 µm.

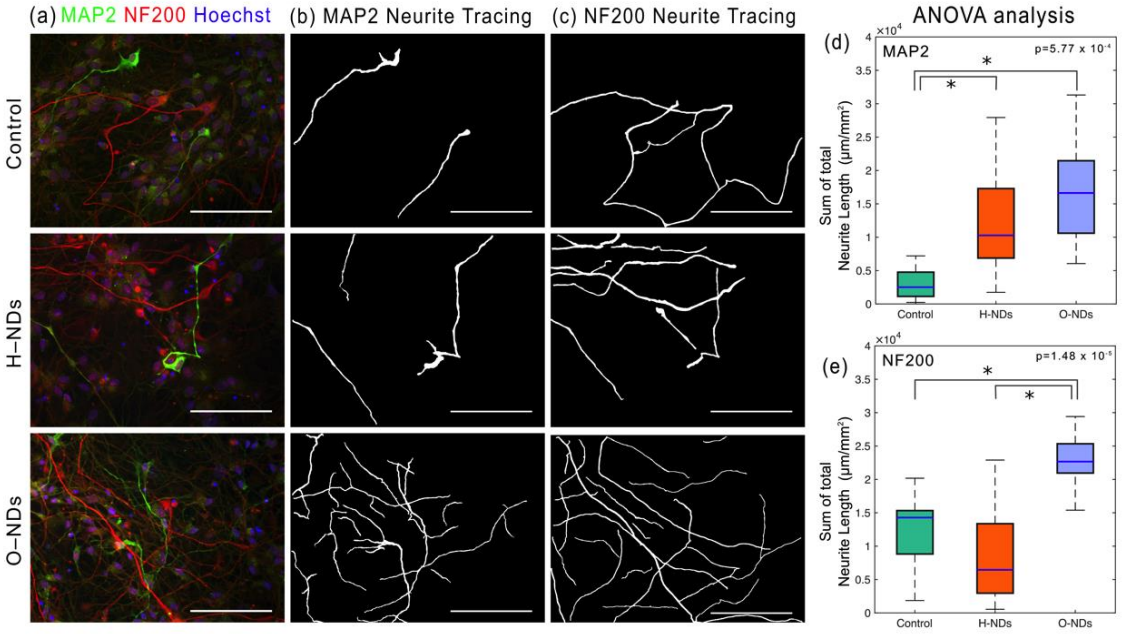

Figure 4 (a) Fluorescently stained images of neurons, which have been spontaneously differentiated from hNSCs after 25 DIV. Neurons have been stained using NF200 (red), MAP2 (green) and Hoechst (Blue). (b + c) Example images after neurite–tracing analysis that has been performed on neurites that have been stained for: MAP2 (b) and NF200 (c). Scale bars 100 µm. (d + e) ANOVA analysis of the sum of total neurite lengths per sample (µm/mm^2). Sample size minimum n=10, p–values for calculated neurite length are shown at the top of each subplot. Confirmation of this significant difference is highlighted using a star.

ANOVA analysis of tracing revealed that neurite extension and length was significantly higher on O–NDs than the glass control and H–NDs. Neurite length expressing MAP2 was calculated to be (1.61x10^4 µm/mm) on O–NDs compared to H–NDs (1.20x10^4 µm/mm) and glass control (3.05x10^3 µm/mm), with an extremely low p–value of 5.77x10^{-4} being observed. Statistical difference was shown between the glass control and both H– and O–NDs, but no difference in H– and O–NDs was shown (Figure 4 b and d). Neurite length expressing NF200 was again highest on O–NDs (2.30x10^4 µm/mm) compared to glass (1.28x10^4 µm/mm) and H–NDs (8.59x10^3 µm/mm). Statistical significance was observed between neurite length of NF200 on O–NDs with the glass control and H–NDs (Figure 4 c + e) p–value 1.48x10^{-5}.

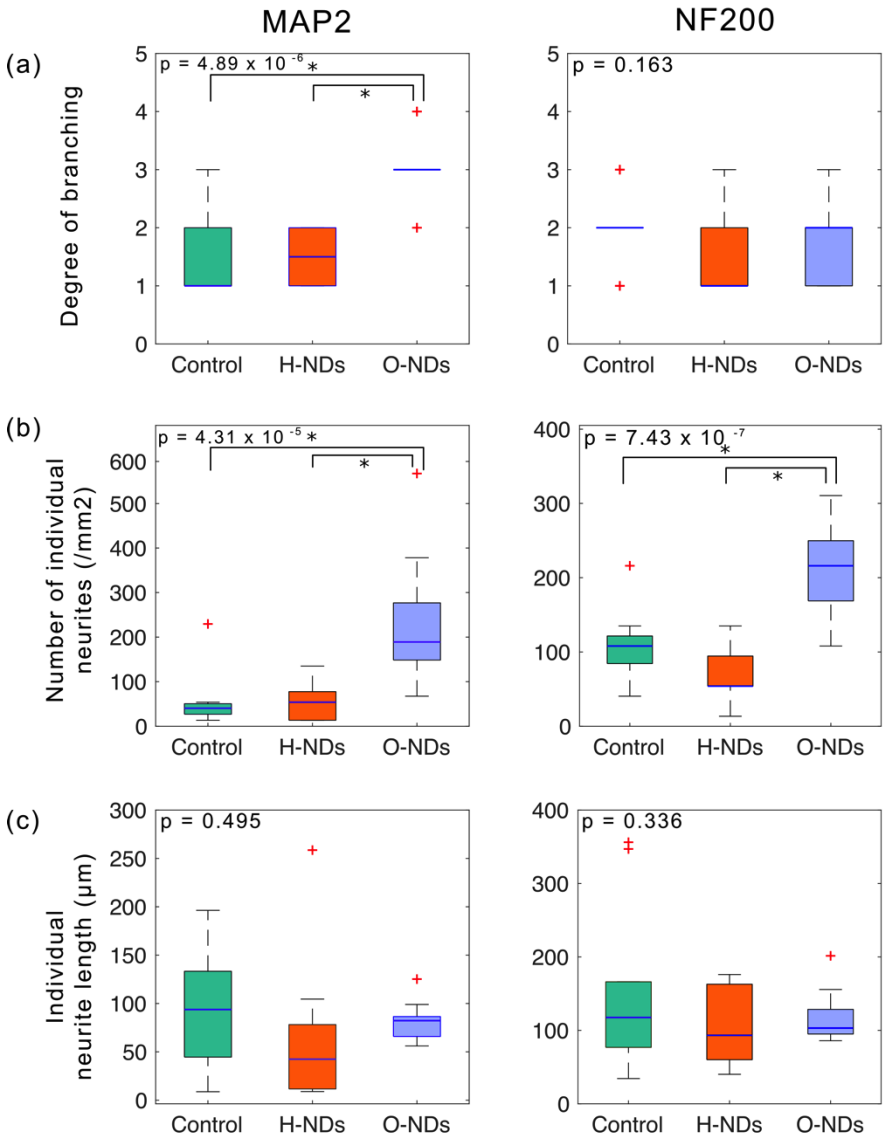

Figure 5 Further ANOVA analysis displayed as a boxplot for the (a) degree of branching observed, (b) the number of individual neurites present (/mm$^{2)}$ and (c) the length of individual neurites, all calculated using SNT on glass, H–NDs and O–NDs for MAP2 and NF200 staining respectively. The medians are shown as a blue horizontal line, boxes represent upper and lower quartiles. Black lines show the range of neurite lengths per stain. Sample size minimum n=10, p–values for calculated neurite length are shown at the top of each subplot. Confirmation of this significant difference is highlighted using a star.

Neurites expressing MAP2 were significantly more branched on O–NDs than the H–NDs and control; as shown in figure 5 a) revealing a p–value of 4.89 x 10^{-6}. No statistical difference was observed for neurites expressing NF200. The density of individual neurites (figure 5 b) was significantly higher on O–NDs for neurites expressing MAP2 and NF200 respectively: (MAP2: 198 /mm^2, NF200: 212 /mm^2) over H–NDs (MAP2: 62 /mm^2, NF200: 73 /mm^2) and control (MAP2: 40 /mm^2, NF200: 105 /mm^2) with corresponding p-values: MAP2 (p–value 4.31 x 10^{-5}) and NF200 (p–value 7.43 x 10^{-7}). For the average length of individual neurites, there was no observable statistical difference between any of the substrates for both MAP2 and NF200 (figure

5 c). These results show that neurites on all three substrates are similar in length but differ in density and degree of branching, with O-NDs being preferable.

RT-PCR

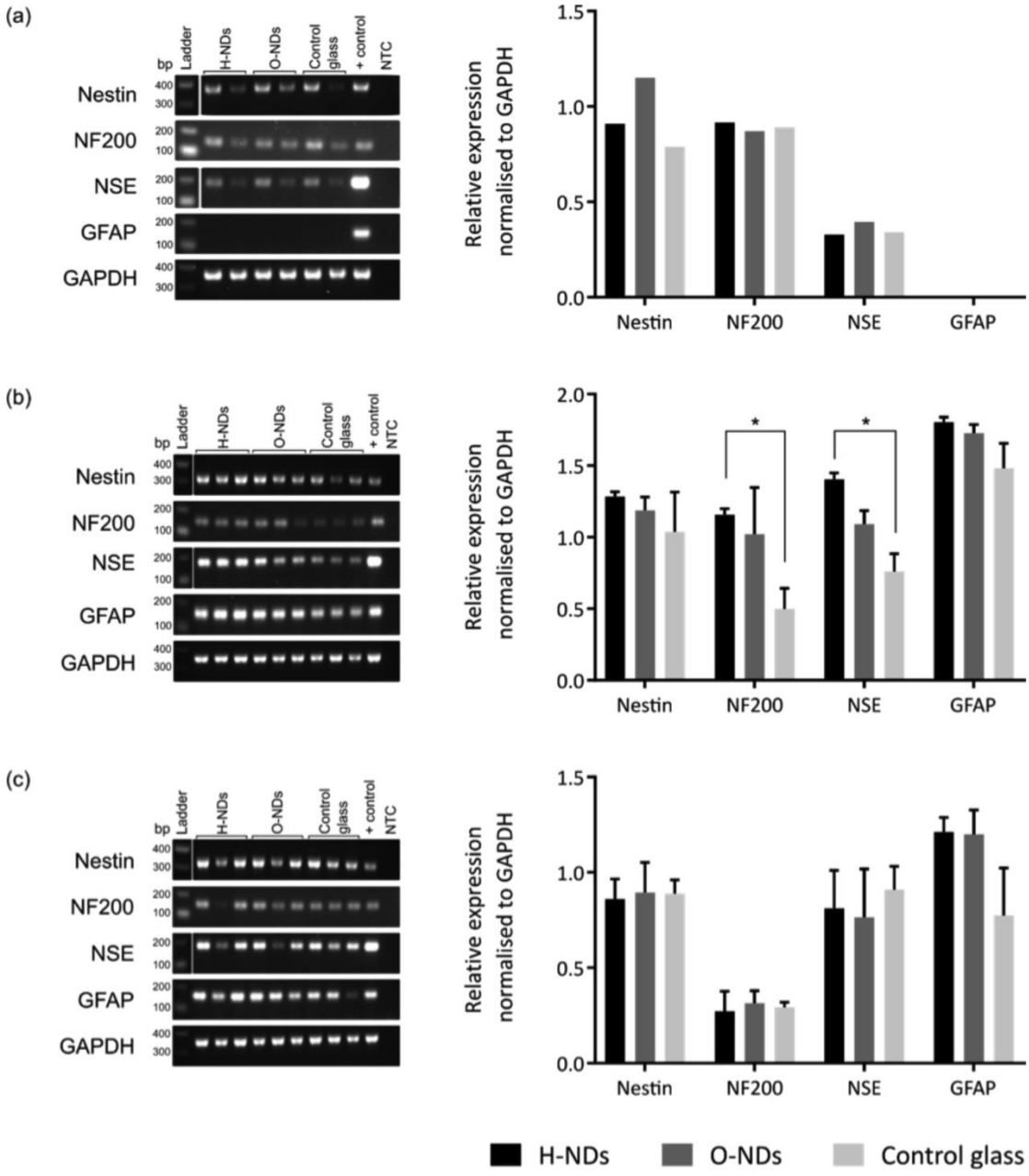

Figure 6 Semi-quantitative PCR analysis of H–NDs, O–NDs and glass control. Human brain (22 weeks post conception) was used as positive control (+control) and water was used instead of cDNA template in the no template control (NTC). GAPDH was used as a reference gene. Data represented as means of band intensity normalised to GAPDH. Plotted as mean ± SEM, two way ANOVA with Tukey's multiple comparisons test. Relative expression of neuronal markers Nestin, NF200, NSE and GFAP was analysed at (a) day 1 of differentiation in biological duplicates, (b) day 10 of

differentiation in biological triplicates and (c) day 22 of differentiation in biological triplicates.

Gene expression was investigated by RT-PCR analysis on hNSCs spontaneously differentiated over H–NDs, O–NDs and glass control at three different time points; day 1 (figure 6 a), undifferentiated hNSCs in growth factor media, day 10 of differentiation (figure 6 b) and day 22 of differentiation (figure 6 c). Human NSCs were found to express neural progenitor marker Nestin, as well as mature neuronal markers NF200 and NSE. After 10 days of differentiation, hNSCs cultured over H–NDs, showed a significantly higher expression of NF200 and NSE over glass control. However, at day 22 of differentiation, no significant difference was observed, suggesting a transient increase in expression of neuronal genes that stabilises as cells become more mature.

Furthermore, GFAP was not expressed in undifferentiated hNSCs, but it was upregulated on all substrates as spontaneous differentiation took place. The expression of GFAP, a typical marker expressed in glial cells, indicates a heterogeneous population of cells and demonstrates the tripotent capacity of hNSCs. Overall, H–NDs and O–NDs showed to have a similar gene expression over 22 days of spontaneous differentiation with a transient higher expression or neuronal markers on the H–NDs compared to glass control on day 10.

Discussion

The ECM environment within the CNS is responsible for many regulatory functions during development and adulthood. The interaction of the ECM and NSCs is critical for cell growth, migration and differentiation, and this is regulated through ECM signalling [35] and changes to matrix stiffness [36]. Therefore, the specific composition and structure of the ECM is vital in controlling the differentiation of NSCs. Cellular adhesion is fundamental in many biological processes as adhered cells are able to sense, interpret and respond to ECM signalling through interactions between focal adhesion sites and receptors at the cell surface [37]. Chemical and physical signals such as: topography, electrostatic charge, hydrophobicity and protein adsorption have critical roles in regulating cell behaviour. Herein, a monolayer of inexpensive NDs produced by a detonation process [38] have been shown to be an excellent substrate for hNSC adhesion, proliferation and differentiation.

During the differentiation of hNSCs into neurons, extensive morphological changes occur. As the cells mature neurites emerge, outgrow, branch and connect with other neurites [39]. This series of morphological changes is vital for facilitating neural network function [40]. Directed and intentional axonal and dendritic outgrowth of neuronal processes is imperative in creating new connection pathways in the CNS [41]. Here, the results achieved show that the spontaneous differentiation of hNSCs on glass, H– and O–NDs resulted in neuron formation, comparable to neurons which have been inductively differentiated into neurons from hNSCs on TCPS at both 25 DIV and 10 PCWs (see figure 2). Here, SNT analysis was used to determine that neurite extension was significantly higher for neurons which spontaneously differentiated on O–NDs. Despite the presence of neurite extension on all three substrates, a significant increase in the length of dendrites and axons was observed on O–NDs. This implies that the functional surface is interacting with the neurons at the nanoscale and is promoting neurite extension, whilst simultaneously maintaining neuron proliferation.

Additionally, the presence of neural markers has been demonstrated by RT-PCR. The longer neurites observed at day 25 on O–NDs do not necessarily translate to a higher expression of NF200 suggesting an indirect correlation between mRNA and protein expression which can be due to the long lifetimes of protein molecules compared to mRNA molecules.

Branching of neuronal dendrites is fundamental for building the central nervous system. The shape and complexity of such neurites occurs during NSC differentiation, enabling the neuron to maximise its spatial coverage and efficiency [42]. Disturbances of dendritic branching during development can result in psychiatric disorders and intellectual disabilities [43]. It is therefore highly beneficial for stem cell transplant therapy if the differentiated neurones are highly branched and extended, as has been observed here on the O–NDs.

It has been shown that O–ND monolayers promote the differentiation of hNSCs into neurons with increased total neurite length, degree of branching and density of neurites. Previous results demonstrate the importance of ND surface hydrophilicity, topography, protein adhesion and surface charge in manipulating hNSC behaviour [27]. O–NDs have successfully induced the differentiation of hNSCs into neurons by mimicking the natural environment of NSCs. It is hypothesised that the NDs have become bio–active upon oxidation and have facilitated extra–cellular signalling between its surface and the hNSCs, mimicking the stem cell niche and promoting neuronal differentiation.

Conclusion

In order to greatly improve tissue regrowth in damaged areas of the brain, implanted materials must induce both endogenous and transplanted NSCs differentiation into neural cells. When stem cells are removed from their *in vivo* niche, they frequently differentiate spontaneously, inefficiently and uncontrollably when subsequently cultured *in vitro* [44]. The potential for use of stem cells in regenerative medicine lies in the ability to be able to control stem cell fate. This can be done via mimicking the microenvironment in which such cells naturally occur [45]. Nano-topography has been demonstrated to be an important factor in regulating stem cell fate. Herein, a facile method for coating glass with nanodiamonds has been described, and the effect of varying surface functionalisation on hNSC adhesion and differentiation has been investigated. It has been shown that the topography of ND monolayers is an exceptional platform for hNSC adhesion, proliferation and differentiation. It should be noted that the NDs were attached through simple sonication from water; a process that is also compatible with a range of 3D substrates – such as polymeric materials – as well as the 2D (glass) used here, making the use of NDs a very versatile platform for neuro-regenerative applications.

The observed preference for neuronal differentiation was confirmed via semi-quantitative PCR and immunocytochemistry of spontaneous differentiated hNSCs, where inducing factors were removed from the culture medium. This is the first time NDs have been used to investigate the spontaneous differentiation of hNSCs, with extremely promising results being shown. It has been discovered that NDs with oxygen functionalisation promoted adhesion and encouraged the differentiation of hNSCs into neurons without exterior factors, with dendritic morphology comparable to those of neurons which have been inductively differentiated on TCPS after both 25 DIV and 10 PCWs. Neurite extension, degree of branching and density of neurites was significantly higher on O–NDs over both H–NDs and the glass control. For example, the total number of neurites and total neurite length expressing MAP2 was over 5 times higher for the O–NDs compared to the control and 2 times higher for neurites expressing NF200. This along with the simple process in which monolayers of NDs are formed, provides significant promise for the application of coating neural implants with O–NDs and as an *in-vitro* substrate for aiding neural stem cell based therapy.

Experimental Section

Nanodiamonds

Monodispersed detonation nanodiamonds (DNDs) (5–10 nm) were used throughout (New Metals & Chemicals Corporation, Tokyo, Japan). This form of DND has been subjected to a de–agglomeration process utilising wet ball milling with zirconia prior to purchase [46]. Herein, all DNDs were subject to a Hydrogen treatment (2.3). An investigation into the effect of ultra–high powered sonication on the agglomeration of these particles was investigated using DLS and AFM.

Nanodiamond monolayer coatings

Nanodiamond monolayer coatings are obtained by ultrasonicating substrates in the H–DND solution (0.05 g/L of NDs) for 10 minutes (excess time). Glass (Cover glass, Menzel–Gläser, Thermo Scientific, UK) was used throughout as the substrate for ND attachment as the transparency allowed for easy optical and fluorescent imaging. Prior to seeding substrates were degreased in acetone, isopropyl alcohol (IPA) and then deionised (DI) water (each for 5 minutes sonication), to remove residue. Characterisation of these monolayer coatings and subsequent Hydrogen and Oxygen termination using XPS, contact angle, protein binding and AFM measurements have been previously reported by Taylor et al. [27].

Hydrogen termination

DNDs were dried by evaporating off excess water at 80°C for 30 minutes. Hydrogen functionalization of these DNDs was achieved using a hydrogen anneal process. A custom–made chamber was used to heat samples to 600°C in 25 Torr of hydrogen for 5 hours and allowed to cool in hydrogen. H–NDs were then re–suspended in DI water (0.05 g/L) and subjected to ultra-high power sonication as aforementioned.

Oxygen termination

Oxygen functionalization of the NDs was achieved using an ozone treatment on H–ND monolayers. A custom built chamber was used in conjunction with a commercially available ozone generation unit (Ozonia TOGC2–100201). Here, samples were subjected to ozone flow at a pressure of 50 mbar, at 200°C for 1 hour. After which the sample was allowed to cool in ozone before being removed.

Dynamic light scattering

A Zetasizer Nano ZS was used to obtain optical particle–size distribution of nanodiamond colloids with a particle range measurements between 1 nm and 1.5 µm being taken. Triplicates of 1 ml at 0.05 g/L of each nanodiamond solution were used, both before and after ultra–high powered sonication using a VCX500 Vibra-cell sonicator with the cup horn accessory (100% amplitude, 3:2 duty cycle, water cooled and temperature controlled to be <30°C, 5 hours) to fully disperse the NDs.

Atomic Force Microscopy

Atomic force microscopy (AFM) measurements were carried out using a Veeco Dimension V instrument with aluminum-coated silicon AFM probes (resonant frequency 190 kHz). The system was operated in tapping mode with a VT-103-3K acoustic/vibration isolation system and a VT-102 vibration isolation table at room temperature in air. AFM was performed on H–ND monolayers. Scan sizes of 2 µm were taken. AFM Images were post processed with a median filter (3 × 3 kernel) using MATLAB 2016a software to remove noise.

human Neural Stem cell Isolation and Culture

All procedures involving human tissue were carried out in accordance with the UKs Human Tissue Act 2006. The hNSCs were isolated and expanded according to the protocol described previously [21,27,47]. Briefly, whole brains from human embryos at

Carnegie stage 17 (approx. 42 days) from consenting patients were provided by a tissue bank under ethical approval (NRES Committee London – Fulham, UK) were collected through the Human Developmental Biology Resource (HDBR, http://hdbr.org) and dissected in cold Neurobasal medium (Gibco). After complete removal of the meninges and blood vessels, the tissue was chopped into smaller pieces and digested in Accutase (Gibco) solution at 37°C for 30 minutes with occasional trituration to obtain single cell suspension. Cells were then centrifuged and re-suspended in growth medium composed of DMEM/F12 with Glutamax TM supplemented with 1% (v/v) penicillin/streptomycin, 1% (v/v) 100× N2 supplement, 2% (v/v) 50× B27 supplement (all Gibco), 20 ng/ml human recombinant FGF2, 20 ng/ml human recombinant EGF (both Peprotech), 50 µg/ml BSA fraction V and 5 µg/ml heparin (both Sigma). Cells were plated on laminin (10 µg/ml, Sigma) – coated dishes and grown for 7 days *in vitro* with the media changed every 2 days to remove any dead cells or debris. To eliminate neurons from the primary cultures and get a homogenous culture of neural stem cells, the cells were first transferred onto 0.1% (w/v) bovine gelatine (Sigma) – coated dishes for 7 days to form neurospheres, which were then re–plated onto laminin–coated dishes for further expansion. For routine expansion and further experiments, cells were grown in growth media supplemented with laminin instead of coating the dishes. Passages up to 30 were used for all experiments.

Spontaneous differentiation of hNSCs

To enabled spontaneous differentiation, 6.5 x 10^4 cells were plated onto 24 well plates containing glass coverslips controls or ND monolayers with both H–and O–termination. Cells were cultured with hNSC medium (normal culture conditions) until day 3, when the growth factors and heparin are removed. The new growth factor free medium was changed every 3–4 days, and the cells were left to differentiate for 22 days. Cells were kept for a total of 25 DIV (3 DIV with hNSC medium and 22 DIV with growth factors being removed), this is summarised in Table 1 below:

hNSC medium (1-3) DIV	Growth factor removal (4-25) DIV
1% P/S	1% P/S
1% N2	1% N2
2% B27	2% B27
50µg/ml BSA V	50µg/ml BSA V
5µg/ml Hep	10µg/ml Laminin
20ng/ml FGF2	
20ng/ml EGF	
10µg/ml Laminin	

Table 1. Outlining the medium change used for the spontaneous differentiation culture.

Immunocytochemistry

For immunocytochemistry, hNSCs were seeded on glass cover slip controls or ND monolayers with both H–and O–termination. The cells were fixed with 4% (w/v) paraformaldehyde (PFA) solution in PBS, pH=7.4 for 15 min at RT prior to immunocytochemical protein detection. After three rinses with PBS the cells were incubated with blocking solution composed of 10% (v/v) FBS, 3% (w/v) BSA in PBS with 0.1-2% (v/v) TritonX-100 for 1h at RT to permeabilize cell membranes. Primary and secondary antibodies were diluted in blocking solution and the incubation times were overnight at 4°C for primary, and 1h at RT for secondary antibodies. Hoechst 33258 (2µg/ml) was added during secondary antibody incubation to counterstain cell nuclei. After final three washes in PBS the coverslips were mounted on slides with an aqueous based mounting medium (Hydromount, National Diagnostics). Primary and

secondary antibodies used can be seen in Table 2 below. Images were acquired using an inverted microscope Olympus IX71 (Carl Zeiss, Jena, Germany) equipped with a Hamamatsu ORCA-ER digital camera (Hamamatsu Corp., Bridgewater, NJ). Image processing was done using Fiji.

a) Primary antibody staining:

Name	Host	Company	Cat. Number	Dilution
Microtubule-associated protein (MAP2)	Mouse	Life Technologies	13–1500	1:200
Neurofilament 200 (NF200)	Rabbit	Sigma	N4142	1:100
Neuronal nuclear antigen (NeuN)	Mouse	Millipore	MAB377	1:100
Doublecortin (DCX)	Rabbit	Invitrogen	48–1200	1:200

b) Secondary antibody staining:

Name	Host	Conjugated Fluorochrome	Company	Cat. Number	Dilution
anti-Rabbit IgG	Donkey	AlexaFluor 594	ThermoFisher Scientific	A-21207	1:500
anti-Mouse IgG	Donkey	AlexaFluor 488	ThermoFisher Scientific	A–21202	1:500

Table 2. (a) Primary antibodies and (b) secondary antibodies used throughout for neuronal fluorescent staining.

Neurite Tracing

Simple Neurite Tracer (SNT) software was used for the analysis of total and individual neurite length, density of dendrites and the degree of branching observed after the spontaneous differentiation culture of hNSCs on glass, O–NDs and H–NDs. SNT is a semi–automated application which is able to trace neurites, construct complex neuronal topology and provide quantitative data on morphology [48]. The software is available as a plugin in open source Fiji software. The SNT was used to measure neurites precisely on fluorescently stained images. MAP2 and NF200 proteins were fluorescently tagged and their neurite extensions were used to compare the maturity of neurones on the three substrates. MATLAB 2016a software was used to perform ANOVA analysis on the neurite lengths, density and degree of branching of each substrate. Neurite tracing was performed on at least 10 images per sample set, taken at random for all fluorescent stains for each substrate type. The images used were at a magnification of 40x due to the increased accuracy of tracing neurite length at a higher magnification.

RNA extraction

TRIzol Reagent was used to extract RNA from hNSCs according to manufacturer's protocol. Briefly, coverslips were placed in a new 24 well plate and 500 ml of TRIzol was added per well to homogenise cells. After adding chloroform, samples were centrifuged to separate the RNA containing aqueous phase from the organic phase. The aqueous phase was carefully removed and isopropanol was added. RNA was then pelleted after centrifugation and washed with ethanol. Samples were pelleted again and the remaining RNA was resuspended in RNase free water.

DNase treatment
To ensure RNA samples were free of genomic DNA, TURBO-DNA-free kit (Life Technologies) was used according to manufacturer's protocol. Briefly, 1 µl of TURBO DNase and 0.1x volume of 10x TURBO DNase Buffer were gently mixed with RNA, followed by an incubation at 37°C for 20-30 minutes. DNase inactivation reagent was added and incubated for 5 minutes at RT. Samples were then centrifuged at 10,000 x g for 1.5 minutes to pellet the inactivation reagent. The supernatant containing RNA was removed and stored at -80°C until further use.

Reverse Transcription
RNA concentration was calculated using a NanoDrop spectrophotometer and 250 ng were mixed with 1 µl of random hexamers (50 µM) (Thermo Fisher Scientific) and water up to 12.5 µl. Samples were annealed at 80°C for 10 minutes. A master mix containing 1 µl of deoxyribonucleotide triphosphate (dNTPs, 0.2 mM) (Bioline), 1 µl of Moloney Murine Leukemia Virus Reverse Transcriptase (M-MLV RT) (200 U/µl), 4 µl of M-MLV RT buffer (5x) and 0.5 µl of RNasin Ribonuclease Inhibitor (2500 U/µl) (all from Promega) was prepared per reaction. Samples were incubated at 30°C for 1 hour to obtain 20 µl of complementary DNA (cDNA) solution. All reactions were performed using a PTC-100 thermal cycler (MJ Research, Inc.).

Polymerase Chain Reaction (PCR)
Primers were designed to span exon-exon junctions, using the free available software Basic Local Alignment Search Tool (https://blast.ncbi.nlm.nih.gov/Blast.cgi) and Primer3web tool (http://primer3.ut.ee/). Primers used for PCR amplification are summarised below in Table 3.

Name	Sequence (5' to 3')	Amplicon size (bp)
Nestin	Forward: CAGCGTTGGAACAGAGGTTGG Reverse: TGGCACAGGTGTCTCAAGGGTAG	389
NF200	Forward: TAGCCGCTTACAGAAAACTC Reverse: AGACTTCTCCACCACTTTGA	155
Neuron specific enolase (NSE)	Forward: CTGATGCTGGAGTTGGATGG Reverse: CCATTGATCACGTTGAAGGC	188
Glial fibrillary acidic protein (GFAP)	Forward: GAAGCTCCAGGATGAAACCA Reverse: ACCTCCTCCTCGTGGATCTT	165

Table 3. List of primer sequences used for PCR amplification.

PCR amplification reactions were performed by mixing 4 µl of 5X Green Go Tag Reaction Buffer, 0.1 µl of GoTaq G2 DNA Polymerase (both from Promega), 1 µl of dNTPs (Bioline), 1 µl of each primer (Sigma), 1 µl of cDNA and 11.9 µl of nuclease-free water for a total of 20 µl per reaction. Cycling conditions consisted of an initial denaturation of 5 min at 95°C followed by 30-32 cycles of denaturation 30 s 95°C, annealing 30 s 56°C, extension 30 s 72°C and a final extension of 7 min 72°C. All reactions were performed in a Veriti Thermal Cycler (Applied Biosciences). No template controls (NTC) were prepared with water instead of cDNA to exclude contamination of the reagents. Glyceraldehyde 3-phosphate dehydrogenase (GAPDH) was used as a reference gene as well as positive controls samples that expressed the gene of interest. Amplified products were analysed by gel electrophoresis using 1.5% (w/v) agarose gels in tri-acetate EDTA (TAE) buffer and 1X SYBR Safe dye (ThermoFisher Scientific). HyperLadder 100bp (Bioline) was used as a molecular weight marker.

Statistical Analysis

For neurite tracing analysis including sum of total length of neurites, degree of branching, number of individual neurites and average individual neurite length fluorescently labelled images were used without any pre-processing. A minimum of n=10 images per sample type and fluorescent marker were used for statistical analysis. A one–way analysis of variance (ANOVA) analysis was performed using Matlab 2016a software which automatically removed outliers and displayed the analysed data as a box–plot. Matlab software was also used to perform statistical significance of ANOVA analysed data and calculate p–values.

Acknowledgements

ACT and RBJ gratefully acknowledge financial support from the EU Framework 7 project 'NEUROCARE' (Project ID: 280433) and the UKs Engineering and Physical Sciences Research Council (EPSRC, EP/F026110/1). CHG and PF thank the Medical Research Council (grant G070089) and The Wellcome Trust (grant GR082557) for financial support.

Author contributions

ACT, CHG, RBJ and PF established the activity, which was carried out by ACT and CHG, supervised by RBJ and PF. ACT and CHG performed the data analysis. All authors contributed to the writing of this manuscript.

References

[1] S. Casarosa, Y. Bozzi, L. Conti, *Mol Cell Ther* **2014**, *2*, 31.
[2] O. Lindvall, R. A. Barker, O. Brüstle, O. Isacson, C. N. Svendsen, *Cell Stem Cell* **2012**, *10*, 151.
[3] E. Arenas, *Biochem. Biophys. Res. Commun.* **2010**, *396*, 152.
[4] C. D. Clelland, R. A. Barker, C. Watts, *Neurosurgical Focus* **2008**, *21*, E9.
[5] S. Temple, *Nature* **1989**, *340*, 471.
[6] D. T. Scadden, *Nature* **2006**, *441*, 1075.
[7] E. Fuchs, T. Tumbar, G. Guasch, *Cell* **2004**, *116*, 769.
[8] F. M. Watt, R. R. Driskell, *Philos. Trans. R. Soc. Lond., B, Biol. Sci.* **2010**, *365*, 155.
[9] L. Little, K. E. Healy, D. Schaffer, *Chem. Rev.* **2008**, *108*, 1787.
[10] M. P. Lutolf, P. M. Gilbert, H. M. Blau, *Nature* **2009**, *462*, 433.
[11] J. S. Robert, *Bioessays* **2004**, *26*, 1005.
[12] G. A. Silva, C. Czeisler, K. L. Niece, E. Beniash, D. A. Harrington, J. A. Kessler, S. I. Stupp, *Science* **2004**, *303*, 1352.
[13] B. Ananthanarayanan, L. Little, D.V. Schaffer, K.E. Healy, M. Tirrell, *Biomaterials* **2010**, *31*, 8706.
[14] N. Li, Q. Zhang, S. Gao, Q. Song, R. Huang, L. Wang, L. Liu, J. Dai, M. Tang, G. Cheng, *Scientific Reports* **2013**, *3*.
[15] Y. J. Li, E. H. Chung, R. T. Rodriguez, M. T. Firpo, K. E. Healy, *J Biomed Mater Res A* **2006**, *79A*, 1.
[16] C.N. Svendsen, M.G. ter Borg, R.J.E. Armstrong, A.E. Rosser, S. Chandran, T. Ostenfeld, M.A. Caldwell, *Journal of Neuroscience Methods* **1998**, *85*, 141.
[17] S.S. Riaz, E. Jauniaux, G.M. Stern, H.F. Bradford, *Developmental Brain Research* **2002**, *136*, 27.
[18] M. Rodrigues, L. G. Griffith, A. Wells, *Stem Cell Research & Therapy 2010 1:4* **2010**, *1*, 32.
[19] B. A. Reynolds, R. L. Rietze, *Nat Meth* **2005**, *2*, 333.
[20] I. Singec, R. Knoth, R. P. Meyer, J. Maciaczyk, B. Volk, G. Nikkhah, M. Frotscher, E. Y. Snyder, *Nat Meth* **2006**, *3*, 801.

[21] Y. Sun, S. Pollard, L. Conti, M. Toselli, G. Biella, G. Parkin, L. Willatt, A. Falk, E. Cattaneo, A. Smith, *Molecular and Cellular Neuroscience* **2008**, *38*, 245.
[22] Y. Wang, H. Deng, Z.H. Zu, X.C. Shen, H. Liang, F.Z. Cui, Q.Y. Xu, I.S. Lee, *Front. Mater. Sci. China* **n.d.**, *4*, 325.
[23] A. Subramanian, U. M. Krishnan, S. Sethuraman, *Journal of Biomedical Science 2009 16:1* **2009**, *16*, 108.
[24] C. G. Specht, O. A. Williams, R. B. Jackman, R. Schoepfer, *Biomaterials* **2004**, *25*, 4073.
[25] P. W. May, E. M. Regan, A. Taylor, J. Uney, A. D. Dick, J. Mcgeehan, *Diamond & Related Materials* **2012**, *23*, 1.
[26] E. M. Regan, A. Taylor, J. B. Uney, A. D. Dick, P. W. May, J. McGeehan, *IEEE J. Emerg. Sel. Topics Circuits Syst.* **n.d.**, *1*, 557.
[27] A. C. Taylor, C. H. González, B. S. Miller, R. J. Edgington, P. Ferretti, R. B. Jackman, *Scientific Reports* **2017**, *7*, 7307.
[28] A. C. Taylor, B. Vagaska, R. Edgington, C. Hebert, P. Ferretti, P. Bergonzo, R. B. Jackman, *J. Neural Eng.* **2015**, *12*, 066016.
[29] W. Yang, O. Auciello, J. E. Butler, W. Cai, J. A. Carlisle, J. E. Gerbi, D. M. Gruen, T. Knickerbocker, T. L. Lasseter, J. N. Russell, L. M. Smith, R. J. Hamers, *Nat Mater* **2002**, *1*, 253.
[30] A. Thalhammer, R. J. Edgington, L. A. Cingolani, R. Schoepfer, R. B. Jackman, *Biomaterials* **2012**, *31*, 2097.
[31] Y.C. Chen, D.C. Lee, T.Y. Tsai, C.Y. Hsiao, J.W. Liu, C.Y. Kao, H.K. Lin, H.C. Chen, T. J. Palathinkal, W.F. Pong, N.H. Tai, I.N. Lin, I.M. Chiu, *Biomaterials* **2010**, *31*, 5575.
[32] Y.-C. Chen, D.-C. Lee, C.-Y. Hsiao, Y.-F. Chung, H.-C. Chen, J. P. Thomas, W.-F. Pong, N.-H. Tai, I.-N. Lin, I.-M. Chiu, *Biomaterials* **2009**, *30*, 3428.
[33] A. E. Nel, L. Mädler, D. Velegol, T. Xia, E. M. V. Hoek, P. Somasundaran, F. Klaessig, V. Castranova, M. Thompson, *Nat Mater* **2009**, *8*, 543.
[34] C. Sanchez, J. Diaz-Nido, J Avila, *Progress in Neurobiology* **2000**, *61*, 133.
[35] S.-H. Kim, J. Turnbull, S. Guimond, *Journal of Endocrinology* **2011**, *209*, 139.
[36] R. G. Wells, *Hepatology* **2008**, *47*, 1394.
[37] R. Flaumenhaft, D.B. Rifkin, *Current Opinion in Cell Biology* **1991**, *3*, 817.
[38] V. N. Mochalin, O. Shenderova, D. Ho, Y. Gogotsi, *Nature Nanotechnology* **2012**, *7*, 11.
[39] D.H. Sanes, T.A. Reh, W.A. Harris, *Elsevier* **2005**.
[40] M.R. Patel, K. Shen, *Cell* **2009**, *137*, 207.
[41] C. Yalgin, S. Ebrahimi, C. Delandre, L. F. Yoong, S. Akimoto, H. Tran, R. Amikura, R. Spokony, B. Torben-Nielsen, K. P. White, A. W. Moore, *Nat Neurosci* **2015**, *18*, 1437.
[42] V.A. Kulkarni, B.L. Firestein, *Molecular and Cellular Neuroscience* **2012**, *50*, 10.
[43] Y.-N. Jan, L. Y. Jan, *Nat Rev Neurosci* **2010**, *11*, 316.
[44] X. H. Parsons, Y. D. Teng, J. F. Parsons, E. Y. Snyder, D. B. Smotrich, D. A. Moore, *Journal of Visualized Experiments* **2011**, e3273.
[45] H. Baharvand, *John Wiley & Sons,* **2014**.
[46] E. Osawa, *Pure Appl. Chem.* **2008**, *80*, 1365.
[47] K. P. U, V. Subramanian, A. P. Nicholas, P. R. Thompson, P. Ferretti, *Biochim. Biophys. Acta* **2014**, *1843*, 1162.
[48] M. H. Longair, D. A. Baker, J. D. Armstrong, *Bioinformatics* **2011**, *27*, 2453.